Intensified Impacts of Central Pacific ENSO on the Reversal of December and January Surface Air Temperature Anomaly over China since 1997

HUA LI,[a,b,c] KE FAN,[b] SHENGPING HE,[d,a] YONG LIU,[b] XING YUAN,[c] AND HUIJUN WANG[a,b]

[a] *Collaborative Innovation Center on Forecast and Evaluation of Meteorological Disasters/Key Laboratory of Meteorological Disaster, Ministry of Education/Joint International Research Laboratory of Climate and Environment Change, Nanjing University of Information Science and Technology, Nanjing, China*
[b] *Nansen-Zhu International Research Centre, Institute of Atmospheric Physics, Chinese Academy of Sciences, Beijing, China*
[c] *School of Hydrology and Water Resources, Nanjing University of Information Science and Technology, Nanjing, China*
[d] *Geophysical Institute, University of Bergen and Bjerknes Centre for Climate Research, Bergen, Norway*

(Manuscript received 24 January 2020, in final form 30 October 2020)

ABSTRACT: The reversal of surface air temperature anomalies (SATA) in winter brings a great challenge for short-term climate prediction, and the mechanisms are not well understood. This study found that the reversal of SATA between December and January over China could be demonstrated by the second leading mode of multivariate empirical orthogonal function analysis on the December–January SATA. It further reveals that the central Pacific El Niño–Southern Oscillation (CP ENSO) has contributed more influence on such a reversal of SATA since 1997. CP ENSO shows positive but weak correlations with SATA over China in both December and January during the pre-1996 period, whereas it shows significant negative and positive correlations with the SATA in December and January, respectively, during the post-1997 period. The CP ENSO–related circulations suggest that the change of the Siberian high has played an essential role in the reversal of SATA since 1997. The pattern of sea surface temperature anomalies associated with the CP ENSO leads to a westward-replaced Walker circulation that alters the local meridional circulation and, further, has impacted the Siberian high and SATA over China since 1997. Moreover, the seasonal northward march of the convergence zone from December to January causes a northward-replaced west branch of the Walker circulation in January compared with that in December. The west branch of the Walker circulation in December and January directly modulates local Hadley and Ferrel circulations and then causes contrasting Siberian high anomalies by inducing opposite vertical motion anomalies over Siberia. The reversal of SATA between December and January, therefore, has been more frequently observed over China since 1997. The abovementioned mechanisms are validated by the analysis at pentad time scales and confirmed by numerical simulations.

KEYWORDS: Atmosphere-ocean interaction; ENSO; Monsoons; Climate variability; Surface temperature; Climate models

1. Introduction

The East Asian winter monsoon (EAWM) dominates the winter climatic anomalies, especially the surface air temperature (SAT) anomalies (SATA) in East Asia/China (Ding et al. 2014; Jhun and Lee 2004). Strong or weak EAWM could give rise to contrasting SATA over East Asia. In particular, the powerful northerly associated with strong EAWM causes cold waves that directly threaten food production (Kiritani 2007; Zhang and Huang 2012) and livelihood. Moreover, frequently occurring haze/smog events that are related to the static stability weather during the weak EAWM years have led to dramatic impacts on human health in East Asia (Lin et al. 2009; Yin et al. 2019; Zhong et al. 2019). The extreme climate events associated with anomalous EAWM could lead to enormous disasters. For example, the worst ice–snow disasters in winter 2008 over South China caused 129 deaths and about USD $21.76 billion economic losses directly (Gao 2009). Most of the current research focuses on the seasonal mean climate, and it has revealed massive evidence and mechanisms related to the changes of winter (December–February) SAT over East Asia. Much evidence suggests that the EAWM/SATA are dominated by the variations of the Siberian high (Liu and Zhu 2020; Lü et al. 2018), the East Asian trough (Wang and He 2012), and the jet stream (Jhun and Lee 2004). Furthermore, the large-scale atmospheric circulations associated with the EAWM/SATA are modulated by remote forcing, such as El Niño–Southern Oscillation (ENSO) (Wang et al. 2000), the sea surface temperature (SST) in the Atlantic (Hao and He 2017), the sea ice over the Arctic (Liu et al. 2012), and the anthropogenic activities (Hao et al. 2019).

In contrast to the variability of seasonal mean SATA that is well studied, the subseasonal variations of winter SATA, which usually causes unexpected disasters in China, have received less attention. For instance, a record-breaking cold event was recorded over East Asia in 2015/16 boreal winter (Geng et al. 2017), but the winter average SAT in this winter showed a positive anomaly because of a remarkable warming spell in December 2015. In fact, the SATA/EAWM experienced frequent subseasonal reversals every winter from 2013 to 2018 (Wang et al. 2013, 2015; Si et al. 2014, 2016). Such subseasonal

Supplemental information related to this paper is available at the Journals Online website: https://doi.org/10.1175/JCLI-D-20-0048.s1.

Corresponding author: Shengping He, shengping.he@uib.no

DOI: 10.1175/JCLI-D-20-0048.1

reverse SATA impose significant challenges for climate prediction over East Asia (Dai et al. 2019; Geng et al. 2017; Lü et al. 2018; X. Xu et al. 2018; Yu et al. 2019).

The underlying mechanisms for the subseasonal reversal of SATA over China are very complex, where the anomalous stratospheric processes (Wang et al. 2013), the blocking high (Si et al. 2014), the ENSO (Wang et al. 2015), the Arctic Oscillation (Si et al. 2016), and the SST over the Atlantic (Zhang and Song 2018) may have contributions. X. Xu et al. (2018) considered the combined effects of the warm phase of the Pacific decadal oscillation, positive central Pacific (CP) ENSO, and the decline in Arctic sea ice on the remarkably cold December and warm January–February. Dai et al. (2019) suggested that the sea ice over different Arctic regions contributes to the SATA variations in different months over Northeast China that eventually led to the reverse SATA between December and January–February. Notably, the subseasonal reversal in the SATA has become more common and frequent in recent years, especially the reversal between December and January.

The subseasonal reversal in the SATA over China might be influenced by remote forcing, such as the SST and sea ice. ENSO is the most prominent climate mode at interannual time scale, exerting remarkable impacts on the East Asian climate in winter (Chen et al. 2013; He and Wang 2013; Wang et al. 2000; Zhang et al. 2015a,b). During the year of El Niño, an anomalous anticyclone at lower levels is located in the western North Pacific, then East Asia often experiences anomalous warm conditions, and vice versa for La Niña (Wang et al. 2000; Wu et al. 2003). The super El Niño events may lead to subseasonal change of winter climate over East Asia. For example, it is revealed that the subseasonal reversal in rainfall anomalies over South China in winter of 1982/83 and 2015/16 (Guo et al. 2018), and the reversal of SATA between December 2015 and January 2016 over East Asia (Geng et al. 2017) were related to the super El Niño.

In addition to conventional ENSO [eastern Pacific ENSO (EP ENSO)], the CP ENSO, which is characterized by a tripole pattern of SST anomalies over the equatorial Pacific (Ashok et al. 2007), has also received considerable concerns in recent years. The CP ENSO and conventional ENSO have different impacts on the global climate (Feng et al. 2016, 2010; Wang et al. 2020; Weng et al. 2009, 2007). For example, the wintertime rainfall over southern China associated with the two types of ENSO is exactly opposite (K. Xu et al. 2018). Yu and Sun (2018) further suggested that the weakening relationship between ENSO and the EAWM was caused by the interference effects of the frequently occurred CP ENSO after the late-1970s. The CP ENSO also has potential impacts on the reversal in SATA at subseasonal time scale (Wang et al. 2015; X. Xu et al. 2018). The CP ENSO may modulate the large-scale atmospheric circulations at subseasonal scales to alter the subseasonal climate over East Asia (X. Xu et al. 2018); on the other hand, the different evolution and variability of the CP ENSO between early winter (November–December) and late winter (January–February) also play an important role on subseasonal climate anomalies over East Asia (Wang et al. 2015; Tian and Fan 2020). Furthermore, the CP ENSO and EP ENSO have been increasing and decreasing, respectively, their interannual variability under the changing climate (Timmermann et al. 2018; Yeh et al. 2009), and the influences of CP and EP ENSO on global climatic intensities and scopes have been changed (Guo and Wu 2019). In the background of increased interannual variability and occurrence of the CP ENSO, the influence of the CP ENSO on the subseasonal variability of winter SATA over China needs further investigation.

Based on the abovementioned, a series of questions arise here: 1) Does the reversal in SATA between December and the following January over China have inherent features and dominant mode? 2) How may we distinguish and demonstrate the mode of reverse SATA? 3) What factors could contribute to the reversal of SATA? To answer these three questions are the main motivation of this study. Especially, in this study we will explore the influences of the CP ENSO on the reversal of SATA at multiple time scales. This paper is arranged as follows: Section 2 describes the datasets and methods. Section 3 presents the results including the intensified relationship between the CP ENSO and reversal of SATA since 1997 (section 3a), the mechanisms for the impact of the CP ENSO on the reversal of SATA since 1997 (section 3b), and the numerical simulations (section 3c). The conclusions and discussion are provided in section 4.

2. Datasets and methods

a. Datasets

We employed global monthly atmospheric reanalysis data for the period of 1961–2017 from the National Centers for Environmental Prediction–National Center for Atmospheric Research (NCEP–NCAR) reanalysis dataset, including the horizontal winds, vertical velocity, and geopotential height with a horizontal resolution of 2.5° × 2.5° and 17 vertical pressure levels (Kalnay et al. 1996). This dataset has been widely applied in climate and weather studies, and it has a long-time coverage. We used a gridded monthly surface temperature observation dataset with a horizontal resolution of 0.25° × 0.25° from more than 2400 observation stations in China (CN05.1) to support the results obtained from the reanalysis dataset (Wu and Gao 2013). SST during the period of 1961–2017 were derived from the National Oceanic and Atmosphere Administration Extended Reconstructed SST, version 5 (NOAA-ERSSTv5), dataset with a resolution of 2.0° × 2.0° (Huang et al. 2017).

b. Numerical simulations and statistical procedures

We conducted the atmospheric generation circulation model (AGCM) experiments by using the Community Atmosphere Model, version 5 (CAM5), to investigate the enhanced impacts of the CP ENSO on the reversal of SATA since 1997. The physical and chemical processes in the CAM5 have been improved compared with previous version (Neale et al. 2012). The CAM5 simulations were performed at a horizontal resolution of 1.9° × 2.5° and 30 hybrid pressure–sigma levels. We have designed three experiments (Table 1). The first one is to force the model with climatological seasonal cycle of global

TABLE 1. Dataset employed in this study and design of the AGCM sensitivity experiments.

Datasets		
CN05.1	NCEP–NCAR-1	NOAA-ERSSTv5
Expt name	Description	
Control run	Climatological mean seasonal cycle of global SST	
emi_pre run	Climatological mean seasonal cycle of global SST plus SST anomalies for warm CP ENSO *during the pre-1996 period* over the region 30°S–50°N, 90°E–80°W from December to the following January	
emi_post run	Climatological mean seasonal cycle of global SST plus SST anomalies for warm CP ENSO *during the post-1997 period* over the region 30°S–50°N, 90°E–80°W from December to the following January	

SST and sea ice (referred to as the control run). It should be noted that the data of the climatological seasonal cycle of global SST used in this model are the model's climatological SST. The second one is a warm CP ENSO run in the pre-1996 period (referred to as the emi_pre run) in which the boundary force consists of the climatological seasonal cycle of global SST with additional anomalous SST over the region of 30°S–50°N, 90°E–80°W from December to the following January. The anomalous SST is obtained by the regression onto the normalized EMI [ENSO Modoki index (EMI); Ashok et al. 2007] during 1961–96. The last one (referred to as the emi_post run) is similar to the emi_pre run, except that the anomalous SST is obtained by the regression onto the normalized EMI during 1997–2016. The atmospheric composition of all three experiments was constant at the level in the year of 2000. All three experiments were integrated for 36 years—the first 10 years were used for the model spinup, and the following 26 years were used for analysis.

Based on section 1, we know that the reversal of SATA that occurred in 2014/15 is related to the CP ENSO. Moreover, previous studies have suggested that the impact of the CP ENSO on the global climate have strengthened in the recent decade due to the increased interannual variability of the CP ENSO (Timmermann et al. 2018; Yeh et al. 2009), which implies that the relationship between the CP ENSO and the subseasonal reversal of SATA might be changed in recent decades. Thus, we employed the sliding correlation to examine the changing relationship between the CP ENSO and the reversal of SATA over China between December and January. Meanwhile, ''bootstrapping'' is used to estimate the relationship between the CP ENSO and the reversal pattern in SATA over China during the different periods. Bootstrapping, which is a statistical method that uses data resampling with replacement, has been widely employed in the field of climate (e.g., Deser et al. 2017). In this study, we generated 1000 bootstrapped samples to verify the relationship between the CP ENSO and the reversal of SATA. We used Student's *t* test to estimate the significance levels and removed the linear trends for all data before the analysis of regression and correlation.

3. Results

a. *The intensified relationship between the CP ENSO and reversal of SATA since 1997*

To distinguish and demonstrate the mode of reverse SATA over China between December and the following January, the multivariate empirical orthogonal function (MV-EOF) analysis is used to identify the inherent reverse SATA and separate the corresponding mode. In this study, an area-weighted correlation coefficient matrix is constructed for the combined SATA over China in December and the following January during 1961–2017 to carry out the MV-EOF. Figure 1 shows the spatial distribution of the first two leading modes of MV-EOF and the corresponding time series. The first and the second modes (MV-EOF1 and MV-EOF2) explain 27.2% and 20.3% of the total variance of the variability in the December–January SATA over China, respectively. The first two leading modes are independent of each other and are statistically distinguished from the rest of the modes according to the rule given by North et al. (1982). The MV-EOF1 denominates the in-phase change in SATA between December and January (Figs. 1a,b), and its time series (PC1) exhibit a clear increasing trend, which is in line with the warming trend over China in winter (Fig. 1e). In contrast, the MV-EOF2 is characterized by the out-of-phase change in SATA between December and the following January, indicating that the cold and warm anomalies in December and the following in January, respectively (Figs. 1c,d). Moreover, the time series of MV-EOF2 (PC2) implies that the subseasonal reverse SATA also displays interannual variability. Interestingly, the PC2 shows positive value in 2015 and negative value in 2016 (note that 2015 refers to December 2014–January 2015), which means that the MV-EOF2 also captures the cold December–warm January pattern in 2014/15 winter (X. Xu et al. 2018) and the warm December–cold January in 2015/16 winter (Geng et al. 2017). It should be noted that in this study we exclude the temperature over the Tibetan Plateau due to its high altitude.

Given the increased interannual variability and occurrence of the CP ENSO during recent decades, the multiscale relationships between the CP ENSO and the reversal of SATA over China between December and January are examined. Here, we employ the sliding correlation between averaged CP ENSO index of December and January (EMI; Ashok et al. 2007) and PC2 of MV-EOF to reveal the impacts of the CP ENSO on the subseasonal variability of winter SATA over China. Figure 2 exhibits that the CP ENSO exerts a significant impact on the reversal of SATA since 1997. It should be noted that the various sliding windows are employed to explore the cutoff point of the changing relationship. The results revealed by various sliding windows show the cu-off point is around 1997 (not shown), and the 1997 is not a special year to dominate the changing relationship between the CP ENSO and the reversal of SATA in recent years.

Furthermore, we confirm the linkage between the spatial distribution of SATA and the CP ENSO during the pre-1996

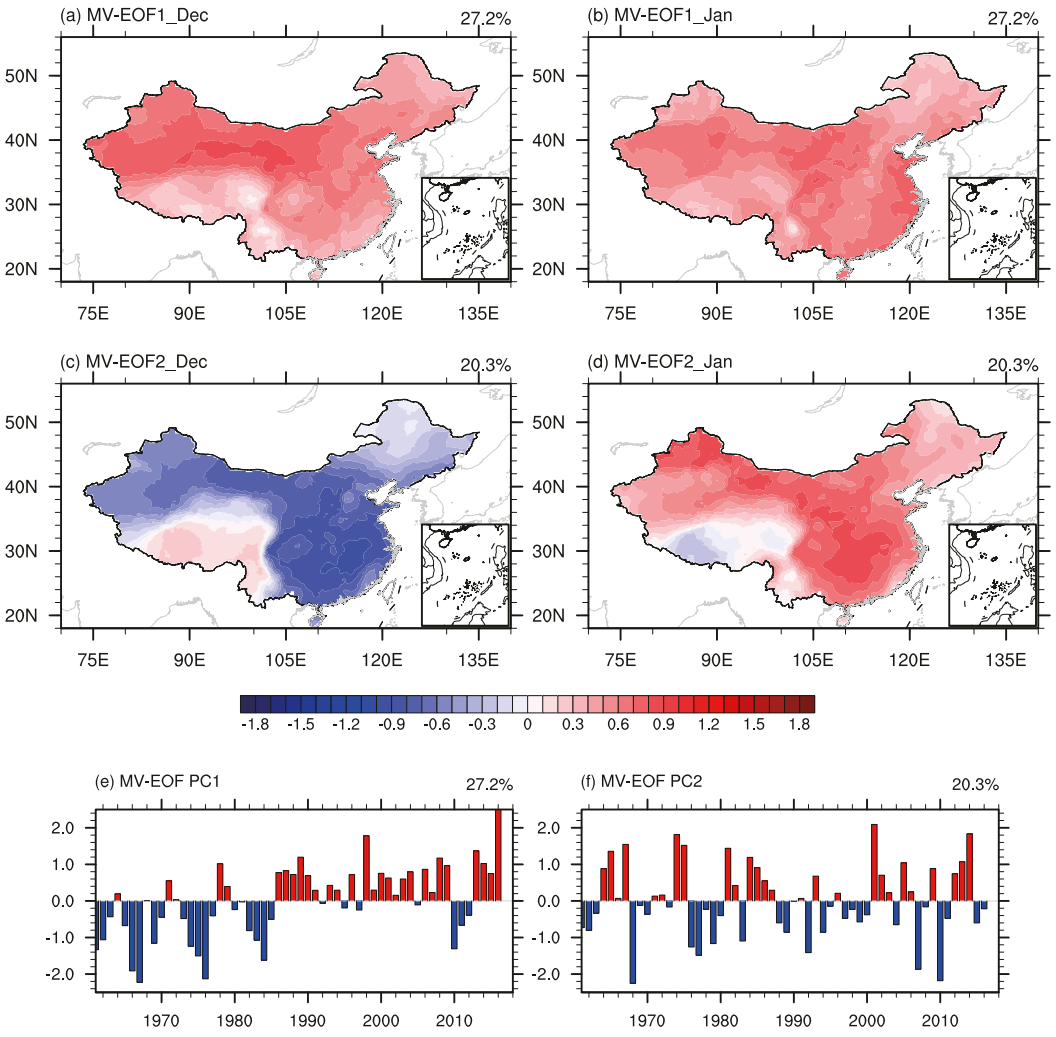

FIG. 1. The first two leading modes of MV-EOF and its time series. SAT spatial distribution in (a) December and (b) January revealed by MV-EOF1. (e) The time series of MV-EOF1. (c),(d) As in (a) and (b), but for MV-EOF2. (f) The time series of MV-EOF2.

(including 1996) and post-1997 (including 1997) periods (Fig. 3), respectively. During the pre-1996 period, the positive CP ENSO causes warm anomalies in southern China in both December and January (Figs. 3a,b). In contrast, the affected areas of the CP ENSO have extended more northward during the post-1997 period. The positive CP ENSO leads to a subseasonal reverse SATA over China between December and January, which exhibits warm SATA in December and the cold SATA in January over most of China (Figs. 3c,d). Previous study has pointed out that the influences of ENSO produces larger uncertainties induced by the atmospheric internal variability (Deser et al. 2017). To further examine the effects of the CP ENSO on the reversal of SATA over China since 1997, the different SATA over China in the CP El Niño events between the post-1997 period and pre-1996 period is analyzed (see the Fig. S1 in the online supplemental material). Compared with the CP El Niño events in the pre-1996 period, the difference also indicates the reversal of SAT between December and January. The significant difference of SAT in December is located in southern China and Northwest China, and the remarkable difference of SAT in January is located in Northeast and Northwest China, those regions are the opposite response

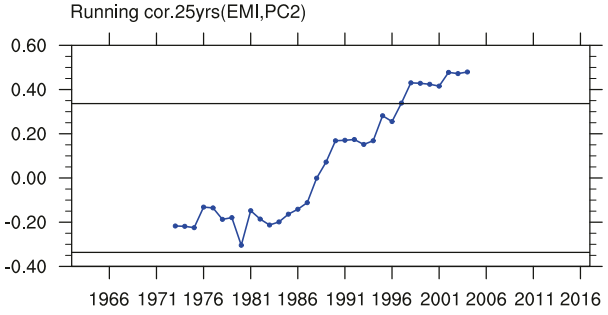

FIG. 2. The 25-yr sliding correlation between EMI and PC2 during 1961–2016. The black horizontal lines denote the 90% confidence level based on the Student's *t* test.

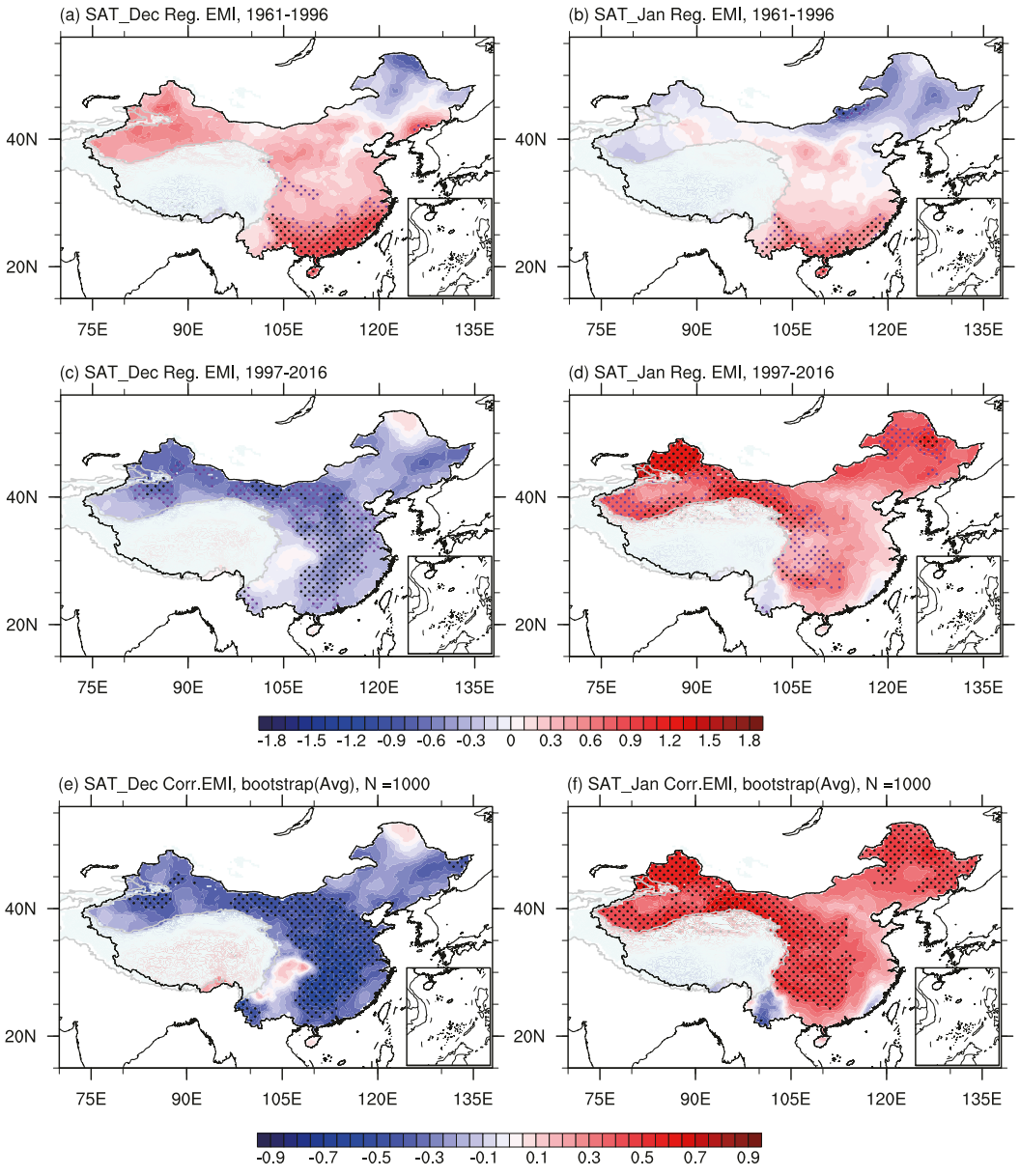

FIG. 3. Regression of SAT onto the normalized EMI in (a) December and (b) January during the pre-1996 period. The regression map of SAT onto the normalized EMI in (c) December and (d) January during the post-1997 period. Correlation coefficients of 1000 bootstrapped samples between the CP ENSO and SAT in (e) December and (f) January since 1997. The purple and black dotted areas denote the 90% and 95% confidence levels based on the Student's *t* test.

regions of the CP ENSO in different periods. Ultimately, we also used the bootstrapping method, which is also employed by Deser et al. (2017), to test the relationship between the CP ENSO and the reversal of SATA since 1997. We have generated 1000 bootstrapped samples for the observational correlation between the CP ENSO and SATA during the post-1997 period. The averaged bootstrapping correlation coefficients are similar to the Pearson correlation (Figs. 3a,b,e,f). Furthermore, the 90th-percentile and 10th-percentile correlation coefficients of 1000 bootstrapped samples are analyzed in December and January, respectively. In December, the 90th percentile indicate the negative correlation between the CP ENSO and SATA over most of China; by contrast, the 10th percentile denotes the positive correlation between the CP ENSO and SATA over most of China in January (Figs. S2a–f). Thus, the results suggest that the relationship between the CP ENSO and SATA over China in both December and January are significantly different from zero. These results further illustrate the strengthening relationship between the CP ENSO and the reversal of SATA between December and January since 1997.

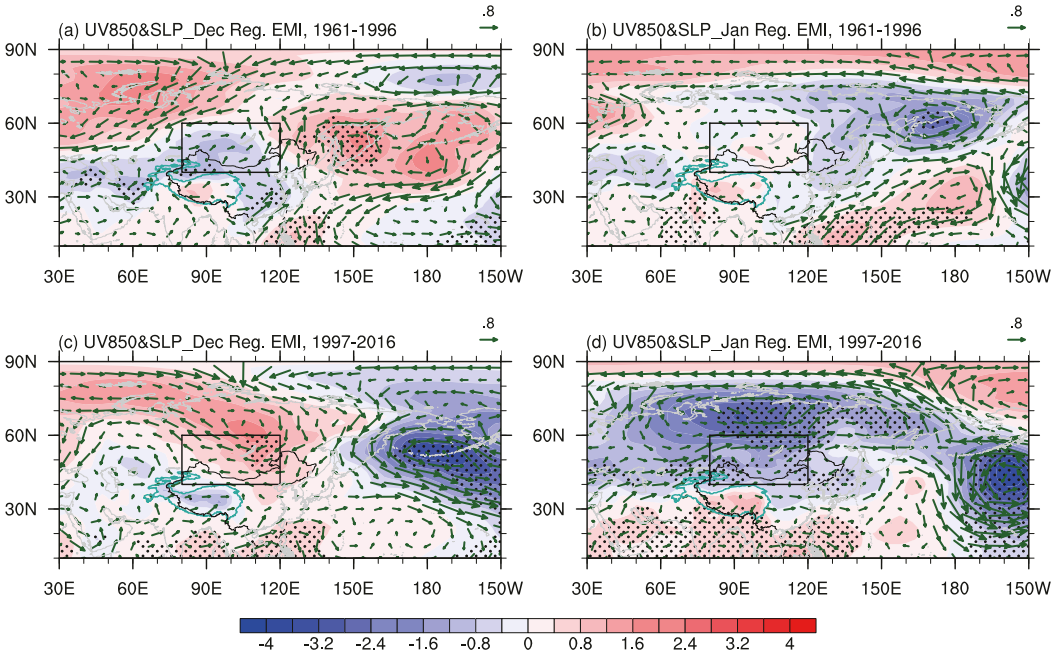

FIG. 4. Regression map of 850 hPa wind field (vectors; unit: $m^2 s^{-1}$) and sea level pressure (colors; unit: gpm) onto the normalized EMI for in (a) December and (b) January during the pre-1996 period. (c),(d) As in (a) and (b), but during the post-1997 period. The black dotted areas denote the 90% confidence level based on the Student's *t* test; the black box denotes the region used to define the SH index.

Meanwhile, to examine whether the CP ENSO also impacts the reversal of SATA over China between December and January at smaller time scales, which could directly induce the extreme temperature events, the CP ENSO–related SATA are analyzed at pentad scales during the pre-1996 and post-1997 periods (see the Fig. S3). The results indicated by pentad scales are similar to the monthly scale. Thus, these results suggest that the CP ENSO could play a crucial role in the reversal of SATA since 1997 both at monthly and pentad scales. It is noteworthy that the anomalies of SAT associated with the CP ENSO exceed 4°C in some special pentads during the post-1997 period, which might give rise to extreme events. At the rest of this study, we will first address the circulation and mechanisms of CP ENSO's impact on the reversal of SATA at monthly scale, then we will check whether the mechanisms at monthly scales are still responsible for smaller time scales (pentad scales).

Furthermore, the CP ENSO–related anomalous sea level pressure (SLP) and atmospheric circulations at 850 hPa are analyzed to reveal different impacts of the CP ENSO between the two periods. In this study, we employ the area-weighted mean SLP (40°–60°N, 80°–120°E) to investigate the intensity of the Siberian high (Wu and Wang 2002). During the pre-1996 period, the Siberian high anomalies related to the CP ENSO in December and January are not significant and weak (Figs. 4a,b), which means that the CP ENSO has limited impacts on the Siberian high. Meanwhile, the CP ENSO–related positive SLP anomalies located over the South China Sea and the Philippines Sea induce the significant southerly anomalies prevailing from the South China Sea to South China, those southerly wind can weaken the northerly wind induced by the EAWM, and then cause the warm anomalies over South China (Fig. 4a). Moreover, the anomalous SLP and wind fields at 850 hPa associated with the CP ENSO in December is similar to that in January during the pre-1996 period (Figs. 4a,b). The anomalous circulations are consistent with the CP ENSO–related SAT anomalies (Figs. 3a,b).

In contrast, during the post-1997 period, the SLP anomalies associated with the CP ENSO between December and January exhibit distinct discrepancies, especially over mid–high latitudes in Eurasia. In December, positive SLP anomalies over Siberia (Fig. 4c) indicate stronger-than-normal Siberian high (Fig. 4c), which is consistent with northerly anomalies over northern China (Fig. 4c). At the same time, a negative SLP anomalies center located in the North Pacific implies that the Aleutian low is deepened, which is accompanied with significant deepening of the East Asian trough (Jhun and Lee 2004; Song et al. 2016). These results suggest the stronger-than-normal EAWM in December, and finally causes the cold conditions over China. However, in January, negative SLP anomalies are remarkable over mid–high latitudes in Eurasia (Fig. 4d), indicating a weaker-than-normal the Siberian high (Fig. 4d). Meanwhile, significant positive SLP anomalies over south of 30°N further favors weaker-than-normal EAWM and warm conditions over China in January (Li and Yang 2010). Therefore, based on the above analysis, the different Siberian high anomalies associated with the CP ENSO between December and January play an essential role in the reversal pattern in SATA over China during the post-1997 period.

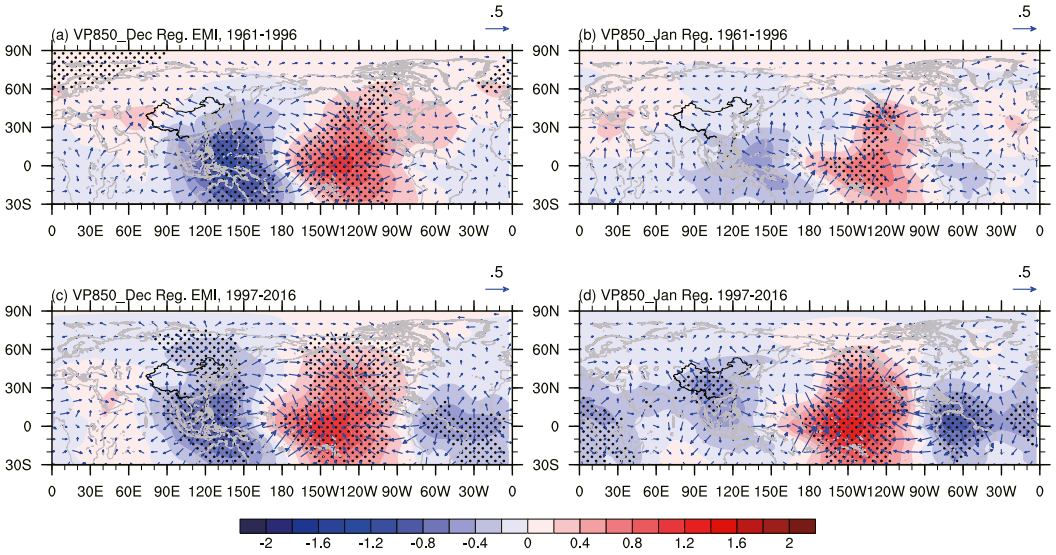

FIG. 5. Regression map of 850 hPa divergent wind (vectors; unit: $m^2 s^{-1}$) and velocity potential (colors; unit: $10^6 m^2 s^{-1}$) onto the normalized EMI during the pre-1996 period for (a) December and (b) January. (c),(d) As in (a) and (b), but for the post-1997 period. The black dotted areas indicate the 95% confidence levels based on the Student's *t* test.

b. Physical mechanisms of the CP ENSO impact on the subseasonal winter temperature reversal over China since 1997

1) MODULATED ROLE BY LOCAL MERIDIONAL CIRCULATION ASSOCIATED WITH THE CP ENSO

The responses of Asian climate anomalies to ENSO are directly attributed to the anomalous Walker circulation and the related anticyclone anomalies around the Philippines (Feng et al. 2010; Wang et al. 2000). The anticyclone anomalies play an important role in bridging the EAWM and ENSO (Yu and Sun 2018). Thus, we also examine the divergent wind, velocity potential and vertical motions to reveal the different responses of the Walker circulation and large-scale divergent motions to the CP ENSO during the two periods. Overall, in both periods of pre-1996 and post-1997, the anomalous Walker circulation features a tripole mode, with descending centers over the tropical western and eastern Pacific and ascending center over the central Pacific. But the strength of vertical motions during the post-1997 period is stronger than that during the pre-1996 period, and the vertical motions are also more significant in the post-1997 period. Meanwhile, the boundary and location of the significant descending motions over the western Pacific associated with the CP ENSO extend more westward in the post-1997 period than in the pre-1996 period. In December, the descending branch of the Walker circulation is located east of 120°E during the pre-1996 period (Fig. 5a), whereas the descending branch of the Walker circulation extends to west of 120°E during the post-1997 period (Fig. 5c). The results are also revealed by the CP ENSO–related vertical motions anomalies averaged along the 10°S–10°N in the two periods (Figs. S4a–d). In the pre-1996 period, the anomalous negative velocity potential over the western Pacific changes from $-2 \times 10^6 m s^{-1}$ in December to $-0.6 \times 10^6 m s^{-1}$ in January, and the anomalous velocity potential becomes insignificant (Figs. 5a,b). These results imply the decreasing Walker circulation anomaly associated with the CP ENSO from December to January. The weakened Walker circulation from December and January is also depicted in the post-1997 period, but the negative velocity potential is still significant in January (Fig. 5d). In addition, the anomalous positive velocity potential also extends westward in the post-1997 period compared to the period of pre-1996 (Fig. 5), which implies the ascending branch of anomalous Walker circulation associated with the CP ENSO also extends westward in the post-1997 period. Similarly, the different vertical motions in the El Niño events between the post-1997 and pre-1996 periods also show the westward replacement of the Walker circulation in the post-1997 period (Figs. S4e,f). These results suggest the CP ENSO–related Walker circulation anomalies, especially its west descending branch, are stronger and more persistent in the post-1997 period than in the pre-1996 period, which can lead to the enhanced relationship between the CP ENSO and subseasonal winter SATA reversal over China after 1997. During the post-1997 period, the difference of significant negative velocity potential of the west branch of the Walker circulation between December and January is also remarkable. Compared with December, the location of significant negative velocity potential center is more northward replacement in January (Figs. 5c,d). The different responses of the western branch of the Walker circulation to the CP ENSO between December and January in the post-1997 period might be the key process to reverse the impacts of the CP ENSO on SATA over China.

The changed Walker circulation/zonal overturning circulations over tropical could alter the local Hadley circulation directly, resulting in the climate anomalies over mid–high

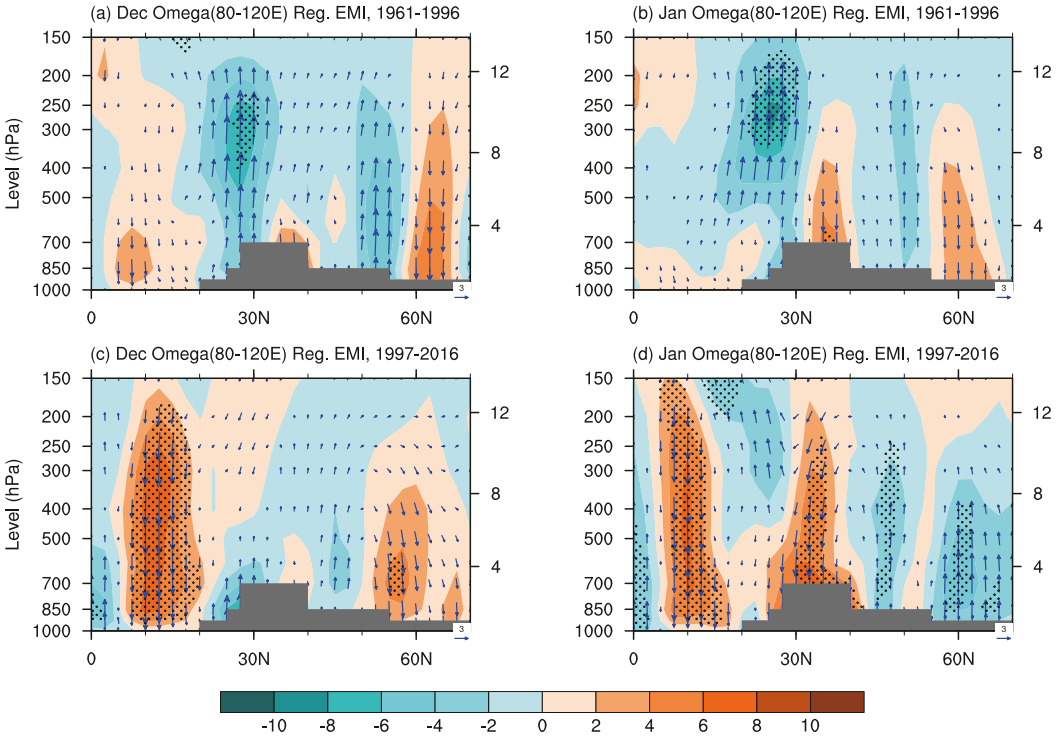

FIG. 6. Regression map of omega (colors; unit: 10^{-3}Pa s^{-1}) and meridional circulation average along 80°–120°E onto normalized EMI during the pre-1996 period for (a) December and (b) January. (c),(d) As in (a) and (b), but for the post-1997 period. The black dotted areas indicate the 95% confidence levels based on the Student's *t* test, and the gray shading indicates the topography.

latitudes by modulating local meridional circulation, such as the Siberian high anomalies (Hsu and Lin 2007; Yu and Sun 2018). Additionally, Wu et al. (2016) suggested that the strength of the Siberian high could be significantly affected by the local vertical motions over Siberia. Figure 6 shows the CP ENSO–related meridional circulation and omega anomalies averaged along 80°–120°E. During the pre-1996 period, insignificant and weak descent anomalies over the tropical eastern Indian Ocean and western Pacific cannot effectively change the local Hadley circulation, thus the signals of the CP ENSO cannot be propagated to mid–high latitudes through local meridional circulation in December and January (Figs. 6a,b). By contrast, the prominent descent over the eastern tropical Indian Ocean and western Pacific significantly weakens the local Hadley circulation during December of the post-1997 period, and then gives rise to a weaker local Ferrel circulation. Subsequently, the weaker Ferrel circulation results in anomalous descending motions over the Siberian region and an enhanced Siberian high (Fig. 6c). Finally, the enhanced Siberian high induces the strong EAWM and cold SATA over China in December. As for the January of the post-1997 period, the significant descending branch of the Walker circulation associated with the CP ENSO extends northward and is located around 30°N (Fig. 6d), which is consistent with the signals revealed by the anomalous velocity potential (Fig. 6d). The northward replacement of the western subsiding branch of the Walker circulation directly intensifies a local Ferrel circulation, then results in the strong ascending branch of Ferrel circulation around 60°N. Ultimately, the enhanced Ferrel circulation causes the weaker Siberian high and warm anomalous SAT over China in January.

To summarize, the anomalous local meridional circulation, which is modulated by the strength and position of the western subsiding branch of the Walker circulation, play an essential role in strengthening the linkage between the CP ENSO and the reversal of SATA between December and January over China since 1997. Furthermore, the stronger, more persistent, and westward replacement of the Walker circulation associated with CP ENSO is responsible for the enhanced impact of the CP ENSO on the SATA over China since 1997. The northward replacement of the western descending branch of the Walker circulation in January compared with that in December is directly associated with the reversal of SATA.

2) POSSIBLE IMPACTS OF CHANGING SST ANOMALIES ASSOCIATED WITH THE CP ENSO

Change of the Walker circulation anomalies associated with the CP ENSO may imply different spatial distribution of the CP ENSO–related SST anomalies (SSTAs). Therefore, we regress the SSTAs in December and January onto the normalized EMI in the two periods (Fig. 7). During the pre-1996 period, the SSTAs associated with the CP ENSO is characterized by anomalous tripole SSTAs pattern in the tropical Pacific, with positive anomalies over central Pacific and

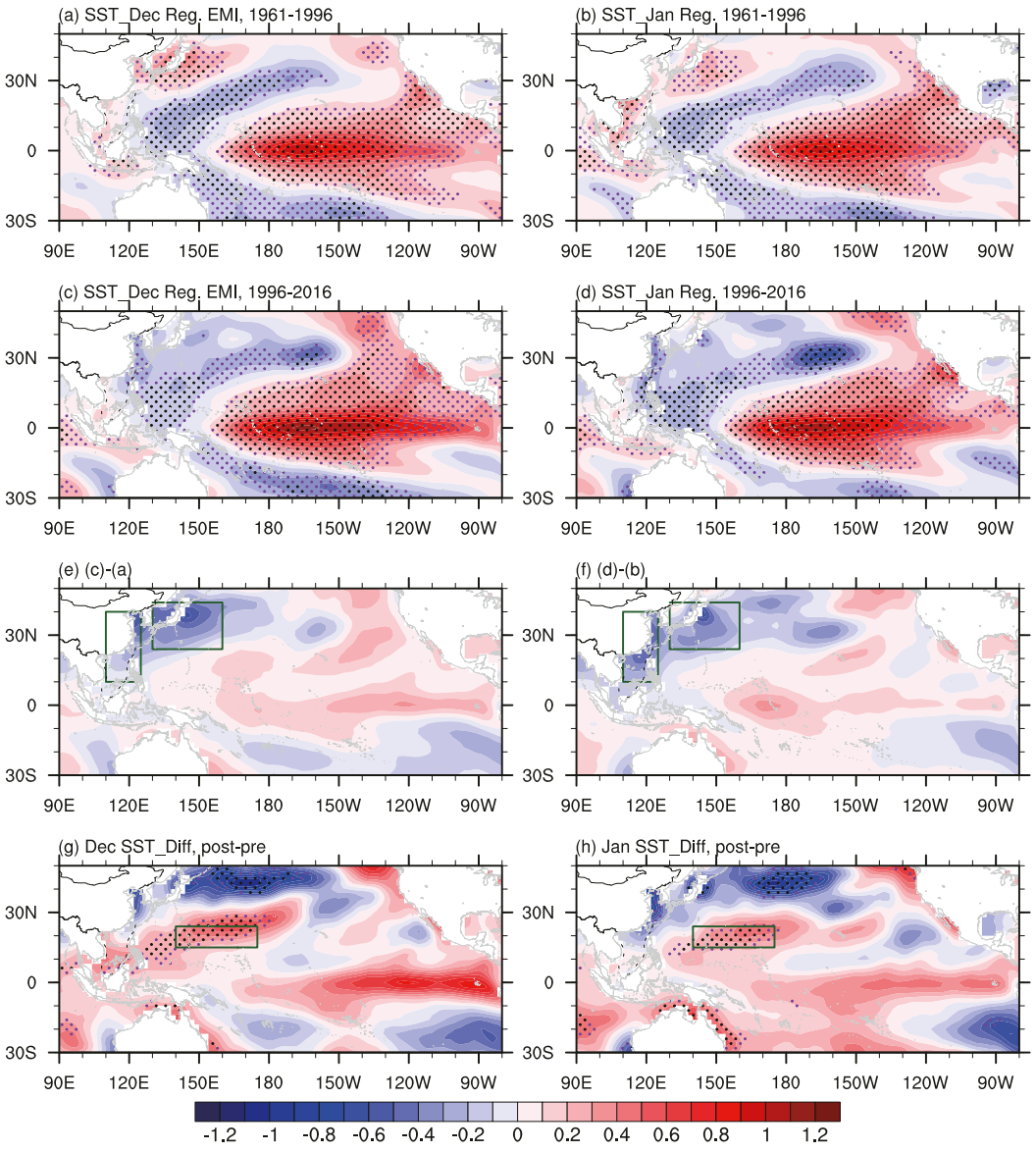

FIG. 7. Regression map of SST onto the normalized EMI during the pre-1996 period in (a) December and (b) January. (c),(d) As in (a) and (b), but for the post-1997 period. (e) (c) minus (a); (f) (d) minus (b). The composited difference of SST of the CP El Niño events between the post-1997 and pre-1996 periods in (g) December and (h) January. The El Niño events are defined by the events exceeding 0.75 times the standard deviation, two standard deviations are obtained by two periods. The two green boxes in (e) and (f) denote the South China Sea region and Kuroshio Extension region in this study; the green box in (g) and (h) indicates the region of the northwest side of the warm anomaly center of the CP ENSO. The purple and black dotted areas indicate the 95% and 99% confidence levels based on the Student's *t* test, respectively.

negative anomalies over the western Pacific and the eastern Pacific. In addition, positive anomalies emerge in the South China Sea and the Kuroshio Extension (Figs. 7a,b). During the post-1997 period, the tropical SST anomalies associated with the CP ENSO are similar to that during the pre-1996 period. However, the CP ENSO–related SSTAs show significant and negative anomaly in the South China Sea and the Kuroshio Extension during the post-1997 period (Figs. 7a,b). The negative anomalies of the regression map of SSTAs between the two periods also show that a distinct difference is the opposite SSTAs over the South China Sea and the Kuroshio Extension (Figs. 7e,f). The negative SSTAs over the western North Pacific associated with the CP ENSO have widened since 1997, so the distribution of SSTAs over the western Pacific has shift from a tripole pattern to a dipole pattern. The widened negative SST over western Pacific anomalies may lead

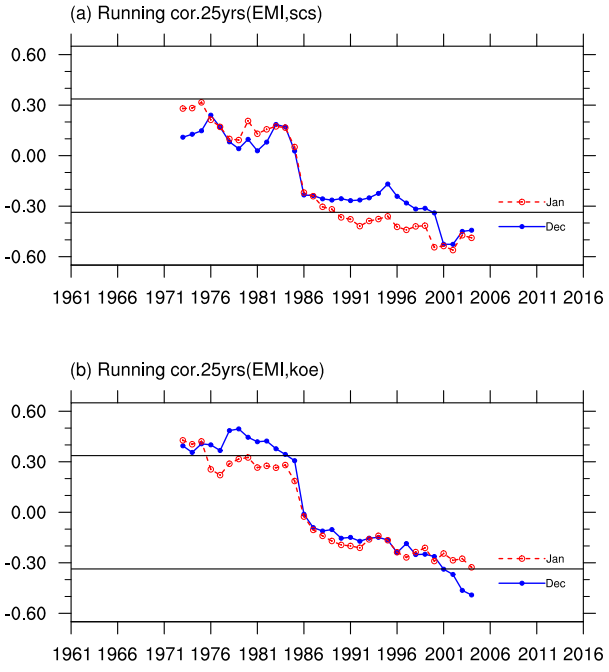

FIG. 8. The 25-yr sliding correlation between the EMI and the SST area-averaged in (a) the South China Sea region (5°–40°N, 110°–130°E) and (b) the Kuroshio Extension region (20°–44°N, 130°–164°E). The horizontal black lines denote the 90% confidence level based on the Student's *t* test, and the blue and red curves indicate the value in December and January.

to a stronger, more persistent, and westward replacement of the west descent branch of the Walker circulation. In addition, the SSTAs over the northwest side of the anomalies center of the CP ENSO also indicate the weakening magnitude of anomalies (the slight positive difference in Figs. 7g,h), the results are clear in the diagram in difference of SST in the CP El Niño events between post-1997 and pre-1996 period (Figs. 7g,h). These changes in SST structure of CP ENSO play a fundamental role in the Walker circulation since 1997.

The local meridional circulation over 80°–120°E is directly affected by the west branch of the Walker circulation. So, we examine the different relationship between SSTAs over western North Pacific and the CP ENSO in two periods. Two indices obtained by area-weighted average SSTAs over the region (5°–40°N, 110°–130°E) and (20°–44°N, 130°–164°E) are used to represent the SSTAs over the South China Sea and the Kuroshio Extension, respectively. The sliding correlation between the EMI and the two SST indices are shown in Fig. 8. Results indicate that the relationship between the CP ENSO and SSTAs over the South China Sea and the Kuroshio Extension have experienced significant interdecadal changes. Before the early and mid-1980s, there is a significant positive correlation between the CP ENSO and two SST indices. Since the mid-1980s, the relationship between CP ENSO and the two indices has been decreasing and shifted from positive to negative correlation. Finally, the negative correlation between the CP ENSO and the two indices became significant around 1997. The transition period is consistent with the enhanced relationship between the CP ENSO and reversal of SATA over China between December and January. The results imply that the anomalous SST pattern associated with the CP ENSO may be an essential factor for the enhanced relationship.

3) BRIDGE ROLE OF DIFFERENT ATMOSPHERIC CIRCULATION BETWEEN DECEMBER AND JANUARY

To explore the causes for the opposite response of SAT anomalies between December and January during the post-1997 period in the background of consistent SSTAs variations, we diagnose the difference in atmospheric circulation between December and January. The differences in 850 hPa wind fields between January and December appear a remarkable discrepancy in both two periods (Figs. 9a,b). The significant westerlies occur over the region from 10° to 30°N, which corresponds well with the northeasterly wind from mid–high latitudes to the convergence north of 20°N (Figs. 9d,e). The stronger convergence at lower levels north of 20°N suggests that there are stronger climatic ascending motions and convection in January than in December. It has been revealed that the enhanced convection contributes to the increased sensitivity of the atmospheric responses to ENSO forcing (Xiang and Wang 2013; Xue et al. 2018). Therefore, the seasonal northward march of convergence zone from December to January may provide an important atmospheric background to reverse SATA responses in December and January to CP ENSO since 1997.

Many studies have suggested that the interdecadal change of climate over East Asia occurs around the late-1990s, thus we also consider whether the different atmospheric circulation in January between the post-1997 and pre-1996 periods also contributes to the enhanced relationship between the CP ENSO and reversal of SATA since 1997. The wind and velocity potential at 850 hPa between the post-1997 and pre-1996 periods cannot describe remarkable differences; thus, the results eliminate the role of interdecadal change in atmospheric circulation between the two periods (Figs. 9c,f).

Meanwhile, analysis of the typical events of the reversal in SATA is helpful for understanding the underlaying mechanism of the CP ENSO's impact on reversal in SATA since 1997, and thus we also examine three typical events of reversal in SATA that occurred in 2007/08, 2010/11, and 2014/15 (Fig. 1f). Most parts of China experienced positive SAT anomalies in December 2007 and 2010 and SAT anomalies in January 2008 and 2011, which was concurrent with negative phase of the CP ENSO. Accordingly, during the positive phase of the CP ENSO, most of China appear the negative SAT anomalies in December 2014 and positive SAT anomalies in January 2015 (see the Fig. S5). The results in these three typical events of the reverse SATA are well consistent with the statistical analysis (e.g., Figs. 3c,d). In addition, we have also checked the local meridional circulation. It is found that the anomalous Ferrel circulation in December–January 2007/08 and 2010/11 is opposite to that in December–January 2014/15 (see Fig. S6), which is also consistent with the reversal of SATA over China.

Furthermore, to examine whether the mechanisms of the CP ENSO impact on reversal in SATA at monthly scales are still

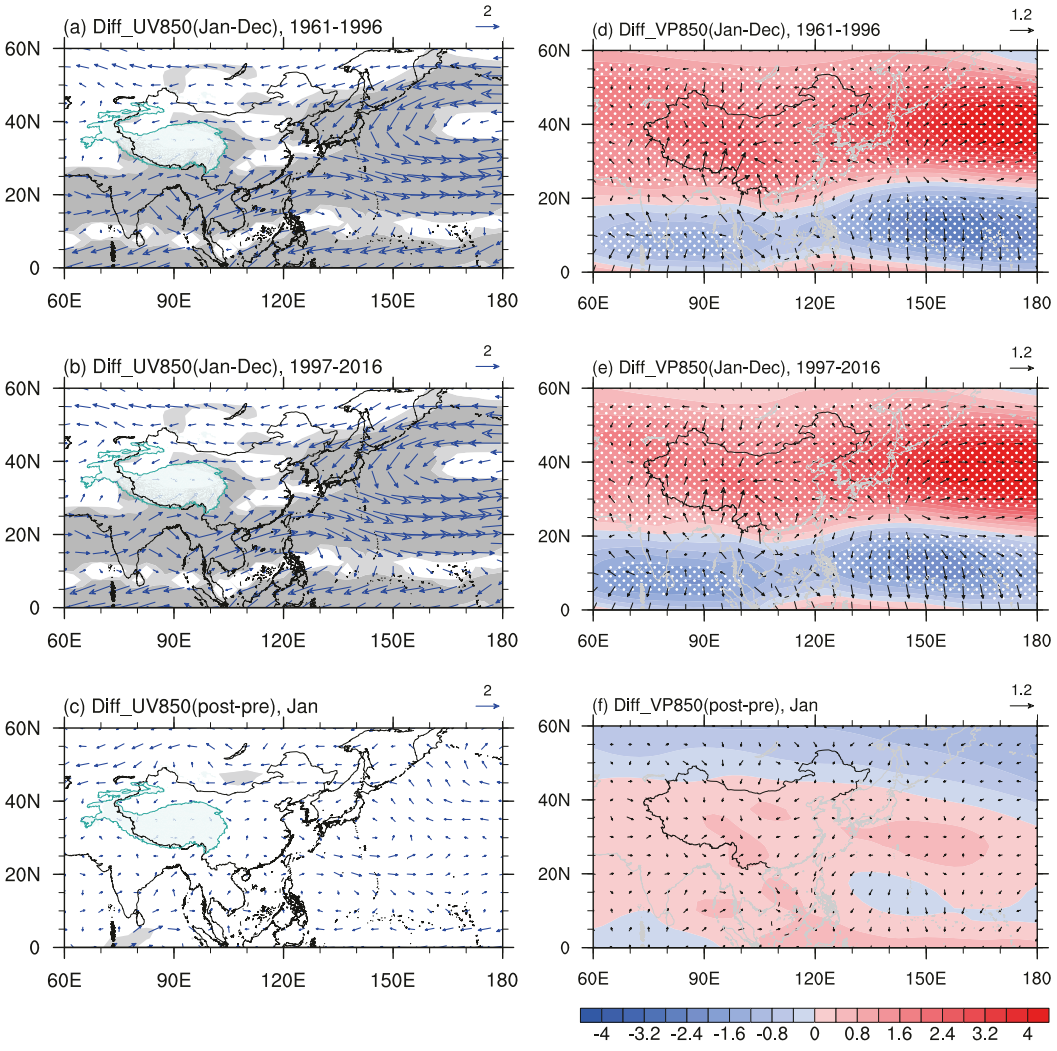

FIG. 9. The different wind at 850 hPa between January and December during the (a) pre-1996 and (b) post-1997 periods. (c) The different wind at 850 hPa in January between the post-1997 and pre-1996 periods; the light and dark shading denote the 90% and 95% confidence levels, respectively, based on the Student's *t* test. The different divergent wind (vectors) and velocity potential (colors; unit: $10^6 m^2 s^{-1}$) at 850 hPa between January and December during the (d) pre-1996 and (e) post-1997 periods; (f) the different divergent wind (vectors) and velocity potential (colors) in January between the post-1997 and pre-1996 periods. The white dotted area indicates the 95% confidence levels based on the Student's *t* test.

responsible for the reversal of SAT anomalies at pentad scales, we analyze the pentad anomalous Siberian high, local Hadley circulation, and Ferrel circulation along 80°–120°E associated with the CP ENSO in the pre-1996 and post-1997 periods. During the pre-1996 period, the weak and positive SATA in both December and January associated with the CP ENSO match the weak and negative Siberian high anomalies (Fig. 10a), and the response of local Hadley and Ferrel circulation to CP ENSO also weak (Fig. 10c). Therefore, these results suggest that the CP ENSO cannot impact the reversal of SATA over China between December and January at pentad scales. By contrast, during the post-1997 period, the SATA associated with CP ENSO exist a remarkable transition from negative to positive in late December. Accordingly, the CP ENSO–related Siberian high anomalies exert a remarkable transition from positive to negative. Thus, the relationship between SAT and Siberian high anomalies is resemblance to the relationship revealed by monthly scales (Fig. 10b). The CP ENSO–related persistent positive local Hadley circulation anomaly during December–January is also similar to results at monthly scales. Meanwhile, the negative local Ferrel circulation anomalies change to positive abruptly in late December, which implies the CP ENSO modulates Ferrel circulation in January directly then induces the reversal of SAT between December and January (Fig. 10d). Thus, these results suggest that the mechanisms revealed by monthly scales are still responsible for the reversal of SATA at pentad scales.

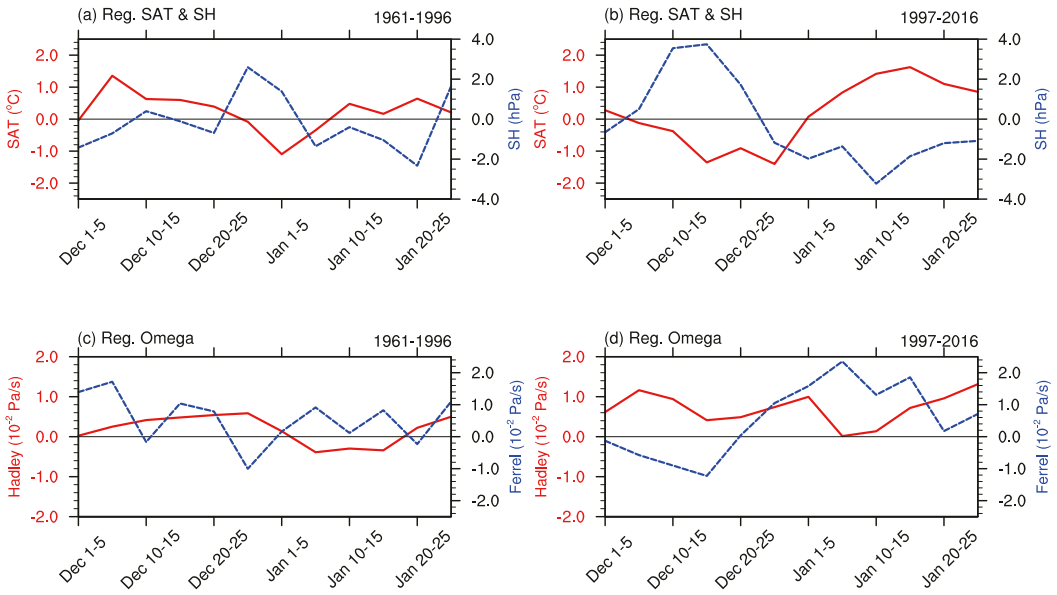

FIG. 10. Regression of pentad area-weighted average SAT over China (omitting the Tibetan Plateau) and SH onto normalized EMI in the (a) pre-1996 and (b) post-1997 period. Regression of pentad local Hadley [denoted by area-weighted omega over the region (80°–120°E, 5°–15°N at 500 hPa) and Ferrel (denoted by area-weighted omega over the region 30°–40°N, 80°–120°E at 500 hPa) downwelling branch onto normalized EMI in the (c) pre-1996 and (d) post-1997 period.

The results from the above indicate that the possible mechanisms of the enhanced relationship between the CP ENSO and the reversal of SATA over China between December and January since 1997 are as follows: the change in structure of SSTAs associated with the CP ENSO since 1997 lead to a westward-extended Walker circulation (especially its west branch), alter the local meridional circulation over 80°–120°E to impact the Siberian high and SATA over China; meanwhile, sensitive response areas to the CP ENSO shift to the north along with the seasonal northward march of convergence zone from December to January. Finally, the different CP ENSO–related west branch of the Walker circulation causes the reversal in SATA over China between December and the following January.

c. *Numerical simulations*

In this section, we employed the AGCM experiments to validate the abovementioned mechanisms. The structure of SSTAs associated with the CP ENSO is an essential process in our mechanisms. Thus, to depict the different distribution of the CP ENSO–related SSTAs in two periods reasonably, we added the SSTAs obtained by regression during the pre-1996 and post-1997 periods on EMI, respectively. Moreover, the extended west branch of the Walker circulation, which is induced by the structure of SSTAs associated with the CP ENSO, is a crucial atmospheric bridge to impact the Siberian high and SATA over China. So, we addressed the composite difference of divergent wind and velocity potential between the control run and two sensitivity runs. In this study, the data of climatological seasonal cycle of global SST used in model are the model's climatological SST, the SST bias might be the primary sources of the model's systemic errors in Walker circulation. Thus, prior to the analysis the results of the model output, we examine the model's systemic errors due to the different Walker circulation between the observation and control experiment. In observations, the boundary between upwelling and downwelling motions of the Walker circulation is around 160°W in both December and January (Figs. S7a,b). In contrast, the boundary between upwelling and downwelling motions of the Walker circulation in control simulations is around 180° in both December and January (Figs. S7c,d). Further, the sensitivity simulations were processed on the basis of control simulation, so the model's systematic errors could influence on the response to the CP ENSO in sensitivity simulations.

In both two sensitivity runs of the warm CP ENSO, the anomalies of the Walker circulation are larger than observed anomalies (Figs. 5 and 11) due to the model's systemic errors. But the responses of the Walker circulation to the CP ENSO in two sensitivity runs show significant difference. In December, the strength of the Walker circulation is stronger, and the west descent branch of the Walker circulation is more westward replacement in the emi_post run compared with the emi_pre run (Figs. 11a,c), the results are consistent with the observation. Then the westward-extended west descent branch of the Walker circulation weakened the Hadley circulation and enhanced the Siberian high. Moreover, in the emi_post run, the center of negative velocity potential anomalies moves to the north from December to January (Figs. 11c,d), which implies that the west descent branch of the Walker circulation is a more northward replacement in January than in December. Then the northward-shifting west descent branch of the

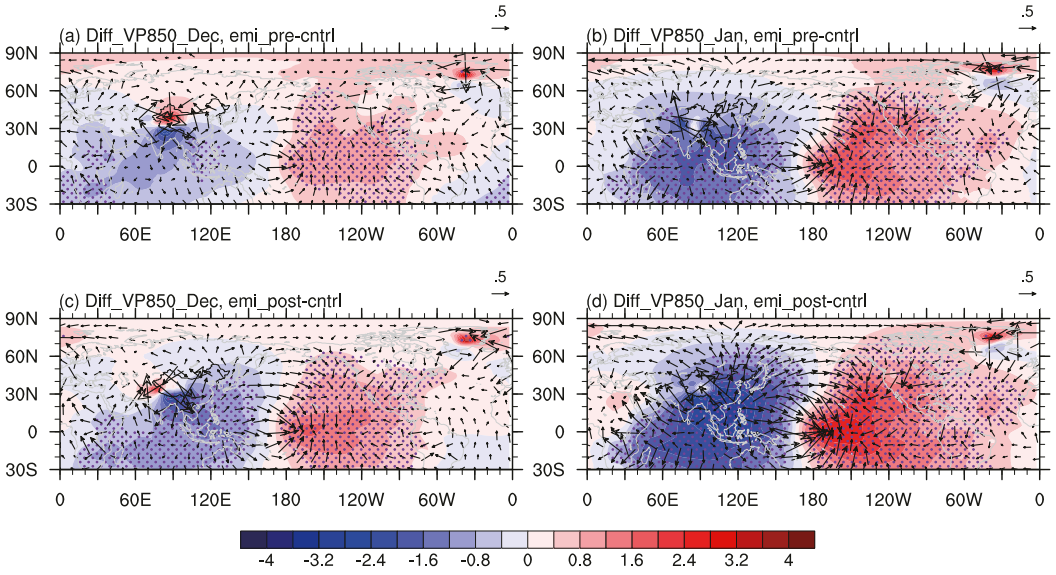

FIG. 11. Composited difference of divergent wind (vectors) and velocity potential (colors; unit: $10^6\,m^2\,s^{-1}$) at 850 hPa in (a) December and (b) January between the emi_pre run and the control run. (c),(d) As in (a) and (b), but for the difference between the emi_post run and the control run. The purple dotted area indicates the 95% confidence level based on the Student's *t* test.

Walker circulation can enhance the Ferrel circulation to decrease the Siberian high in January. Therefore, the forcing SSTAs, which are described by the change in pattern of SSTAs, can roughly reproduce the key physical process during the post-1997 period.

Figure 12 shows the composited difference of SAT between two sensitivity experiments and control run. In the emi_post run, the SATA over most of China shows significant negative anomalies in December, while the remarkable positive SAT anomalies exert over most of China in January (Figs. 12c,d). The Walker circulation increased from December to January in the control simulations (see the Fig. S7), which might be a reason to induce a stronger responses of the Walker circulation to the CP ENSO in January than December, then caused the insignificant difference of SAT in January in sensitivity experiments. In the emi_pre run, significant negative SAT anomalies are located in South China in December due to the model's systemic enhanced Walker circulation and weak responses of SAT in January. To further reveal the results from the AGCM between two sensitivity experiments, the difference of SAT between the emi_post and emi_pre runs in December and January are analyzed (see the Fig. S8). Compared with the emi_pre run, the most part of China describe a cooling and a warming difference of SAT, respectively, in December and January. The difference of SAT between the two sensitivity experiments also implies the intensified relationship between CP ENSO and the reversal of SATA over China in the emi_post run relative to the emi_pre run. Thus, the results in emi_pre are not consistent with the observed SAT, but the difference between emi_pre and emi_post results suggest the intensified impacts of the CP ENSO on the reversal of SATA since 1997.

4. Conclusions and discussion

SATA dominate the winter climate over China, and extreme and volatile SATA results in severe disasters. The subseasonal reversal of the SATA over China, which receives less attention, becomes frequent and raises a great challenge for climate prediction. In this study, we explore the mechanism on the reversal in SAT anomalies between December and the following January over China by investigating the impacts of the CP ENSO on the reversal of SATA.

First, we employ the MV-EOF on winter SATA over China and find that the second leading mode of MV-EOF is associated with the reversal of SATA. The MV-EOF2 explain 20.3% of the variance of the variability in the December–January SAT over China. Meanwhile, the PC2 revealed by MV-EOF shows that a great interannual variability dominates the change of the reversal of SATA. Subsequently, we explore the multiscale relationships between the CP ENSO and the reversal of SATA. Along with the enhanced interannual variability of the CP ENSO in recent years, the relationship between the CP ENSO and the reversal of SATA has been intensified; ultimately, the relationship has become significant since 1997 (Figs. 2 and 14). The schematic diagram of possible physical processes regarding the intensified impacts of the CP ENSO on the reversal of SATA is shown in Fig. 13. The CP ENSO–related SATA in the pre-1996 and post-1997 periods also validates the enhanced relationship (Fig. 3). The circulation anomalies associated with the CP ENSO in the pre-1996 period show that the CP ENSO could impact the SATA only over South China, with similar influence for both December and January. Meanwhile, the responses of the climate system are also weak and insignificant in this period. By contrast, the CP

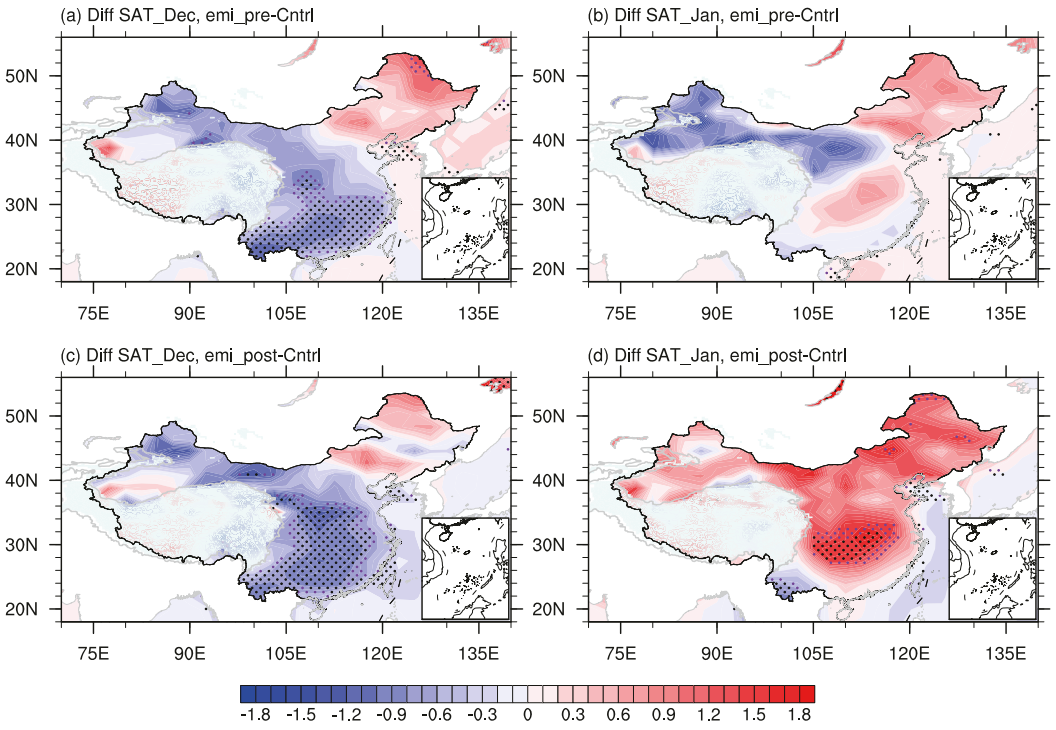

FIG. 12. Composited difference of SAT in (a) December and (b) January between the emi_pre run and the control run. (c),(d) As in (a) and (b), but for the difference between the emi_post run and the control run. The purple and black dotted areas indicate the 90% and 95% confidence levels, respectively, based on the Student's *t* test.

ENSO could influence the SAT over most areas of China in the post-1997 period and induce the opposite responses of SATA in December and January (Figs. 3c,d). Moreover, the circulation anomalies reveal that the contrasting Siberian high anomalies associated with the CP ENSO are crucial processes that cause the reversal of SATA (Figs. 4c,d).

The Walker circulation is directly influenced by the CP ENSO. Compared with the pre-1996 period, the west descent branch of the Walker circulation associated with the CP ENSO extends to the west of 120°E, then could impact the Siberian high via local meridional circulations in the post-1997 period (Figs. 5 and 6). Specifically, in warm CP ENSO years during the post-1997 period, the west descent branch of the Walker circulation weakens the local Hadley circulation, then leads to a weaker Ferrel circulation and enhances Siberian high via descending motions, and finally gives rise to the cold SATA over China in December. In January, the seasonal northward-marching convergence zone causes the west descent branch of the Walker circulation to move to the north at about 30°N, then directly enhances the local Ferrel circulation and weakens the Siberian high by ascending motion, and finally causes the warm SATA over China. In cold CP ENSO years, the opposite has occurred. Furthermore, the CP ENSO–related SSTAs suggest that the westward replacement of the west branch of the Walker circulation is closely associated with structure of SSTAs over the western Pacific. The negative correlated SSTAs has widened over the western Pacific since 1997, and the widened negative correlated SSTAs over the western Pacific leads to the extended west branch of the Walker circulation during the post-1997 period. In addition, the mechanisms revealed by monthly scales are still responsible for the reversal of SATA at pentad scales (Fig. 10). The two sensitivity experiments, which are driven by SSTAs associated with the CP ENSO in the pre-1996 and post-1997 periods, respectively, can roughly reproduce the above process and further validate our mechanisms. In the future, the additional experiments will be forced by observed pattern of the CP ENSO–related SSTAs using the technique of pacemaker for providing more information about the impacts of the different pattern of SSTAs on global climate.

The intensified impacts of the CP ENSO on the reversal of SATA may be modulated by the changing ENSO variations. The pace of increased interannual variability of the CP ENSO, calculated by 25-yr sliding standard deviations, coincides closely with the increased correlation coefficient between CP ENSO and the PC2 (Fig. 14a). The increased standard deviations of SSTAs imply an increase in the number of the CP ENSO events, especially during the post-1997 period (Fig. 14b). Previous studies have pointed out that interdecadal ENSO's variation could affect its global teleconnections (Ashok et al. 2007; Guo and Wu 2019; Ogata et al. 2013; Xie et al. 2010). The increased occurrence of the CP ENSO begins around early and the mid-1980s (Yeh et al. 2009; Yu and Sun 2018), which is the same period when the relationship between the CP ENSO and

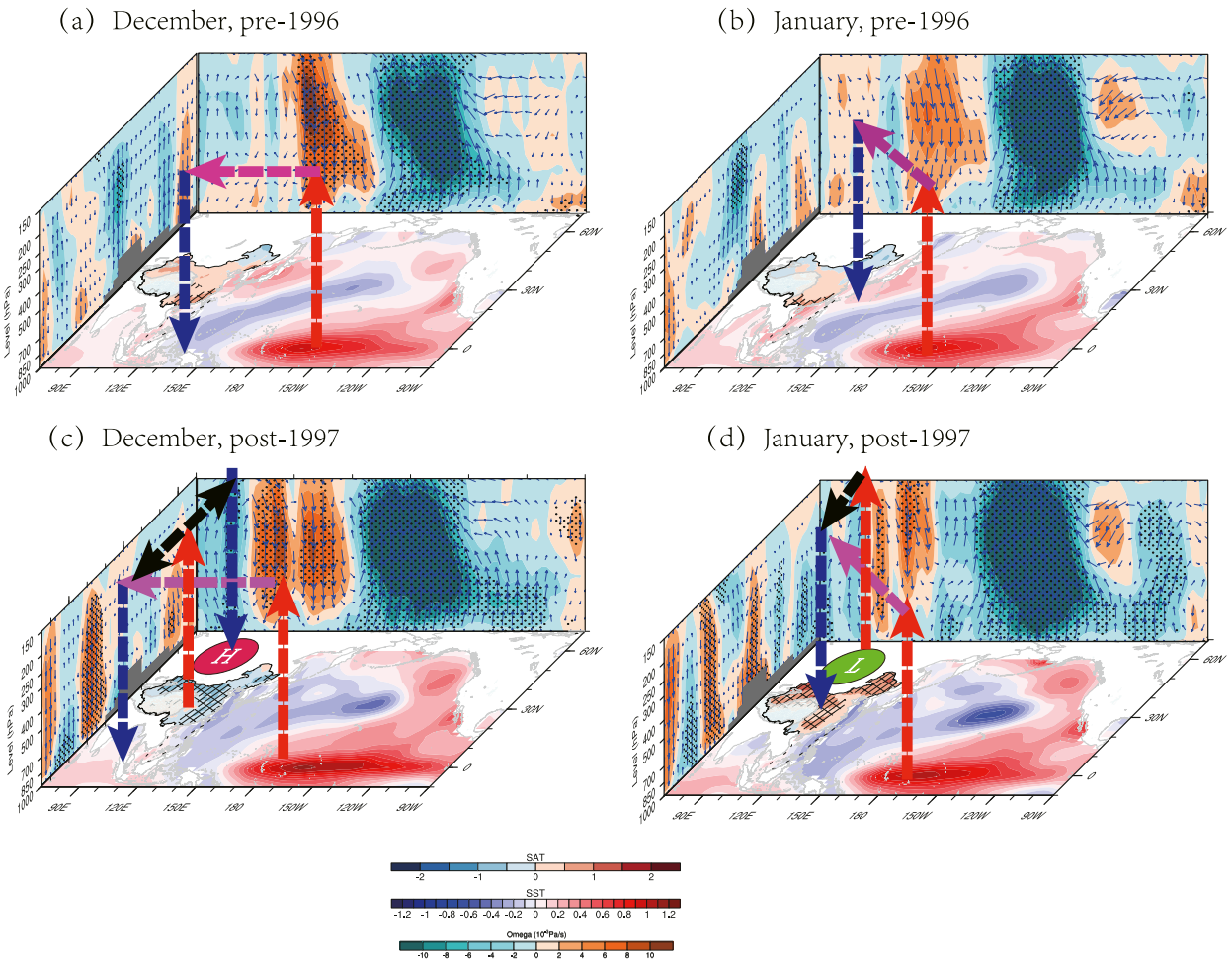

FIG. 13. Schematic diagram of the CP ENSO impacting the reversal SATA in December and January over China. The purple and green ellipses denote the strong and weak Siberian high, respectively.

the western Pacific SSTAs shift to negative correlation from positive correlation rapidly (Fig. 8). Moreover, McPhaden et al. (2011) suggested that the increased occurrence of the CP ENSO is associated with anomalous thermocline depth over the tropical Pacific. So, the anomalous thermocline depth would change the CP ENSO–related SST anomalies by thermocline feedback. There may exist an intrinsic feedback between the frequency of the CP ENSO and its related SST anomalies over the western Pacific, but the underlying mechanism needs further investigation based on the latest dataset of CMIP6 and other large ensemble experiments. In short, the enhanced interannual variability of the CP ENSO plays an important role in enhancing the relationship between the CP ENSO and the reversal of SATA since 1997, and more frequent reversal of SATA over China between December and January may occur in the future due to a more likely occurrence of the CP ENSO under greenhouse warming.

In this study, we have investigated the changing relationship between the CP ENSO and the reversal pattern of December and January SATA over China, and the results show that the Siberian high plays an essential role in the changing relationship. It is noteworthy that the intraseasonal change of Siberian high might be potentially related to the preexisting surface temperature anomalies over Siberia and the stationary Rossby wave train across the Eurasian continent (Takaya and Nakamura 2005). Additionally, the East Asian trough could also impact the Siberian high via large-scale anomalous vertical motion around the rear of the East Asian trough (Ding and Krishnamurti 1987; Song et al. 2016). All components of the East Asian winter monsoon—for instance, the Siberian high, the East Asian trough, and the Aleutian low—have direct or indirect interaction due to their connections with the quasi-stationary planetary waves that are excited and altered by the topography and the diabatic heating (Bozkurt et al. 2019; Held et al. 2002; Chen and Trenberth 1988a,b). Thus, this study cannot rule out the effect of the East Asian trough, which might be addressed in the future.

Acknowledgments. This research was supported by the National Natural Science Foundation of China (Grant 41730964), the Major Program of the National Natural Science Foundation of

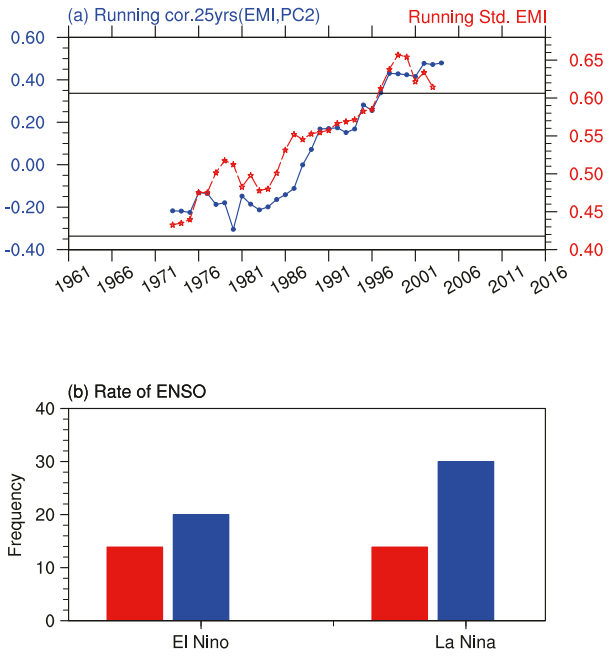

FIG. 14. (a) The 25-yr sliding standard deviations of EMI (red line) and the 25-yr sliding correlation coefficient between MEI and PC2 (blue line) during 1961–2016. (b) The frequency of occurrence of CP ENSO events in two periods; the red and blue bars denote the frequency during the pre-1996 and post-1997 periods, respectively.

China (Grant 41991283), the National Natural Science Foundation of China (Grant 41875118), and the Startup Foundation for Introducing Talent of NUIST.

REFERENCES

Ashok, K., S. K. Behera, S. A. Rao, H. Weng, and T. Yamagata, 2007: El Niño Modoki and its possible teleconnection. *J. Geophys. Res.*, **112**, C11007, https://doi.org/10.1029/2006JC003798.

Bozkurt, D., Y. Ezber, and O. L. Sen, 2019: Role of the East Asian trough on the eastern Mediterranean temperature variability in early spring and the extreme case of 2004 warm spell. *Climate Dyn.*, **53**, 2309–2326, https://doi.org/10.1007/s00382-019-04847-5.

Chen, J., Z. Wen, R. Wu, Z. Chen, and P. Zhao, 2013: Interdecadal changes in the relationship between southern China winter-spring precipitation and ENSO. *Climate Dyn.*, **43**, 1327–1338, https://doi.org/10.1007/s00382-013-1947-x.

Chen, S., and K. E. Trenberth, 1988a: Orographically forced planetary waves in the Northern Hemisphere winter: Steady state model with wave-coupled lower boundary formulation. *J. Atmos. Sci.*, **45**, 657–681, https://doi.org/10.1175/1520-0469(1988)045<0657:OFPWIT>2.0.CO;2.

——, and ——, 1988b: Forced planetary waves in the Northern Hemisphere winter: Wave-coupled orographic and thermal forcings. *J. Atmos. Sci.*, **45**, 682–704, https://doi.org/10.1175/1520-0469(1988)045<0682:FPWITN>2.0.CO;2.

Dai, H., K. Fan, and J. Liu, 2019: Month-to-month variability of winter temperature over Northeast China linked to sea ice over the Davis Strait–Baffin Bay and the Barents–Kara Sea. *J. Climate*, **32**, 6365–6384, https://doi.org/10.1175/JCLI-D-18-0804.1.

Deser, C., I. R. Simpson, K. A. McKinnon, and A. S. Phillips, 2017: The Northern Hemisphere extratropical atmospheric circulation response to ENSO: How well do we know it and how do we evaluate models accordingly? *J. Climate*, **30**, 5059–5082, https://doi.org/10.1175/JCLI-D-16-0844.1.

Ding, Y., and T. N. Krishnamurti, 1987: Heat budget of the Siberian high and the winter monsoon. *Mon. Wea. Rev.*, **115**, 2428–2449, https://doi.org/10.1175/1520-0493(1987)115<2428:HBOTSH>2.0.CO;2.

——, and Coauthors, 2014: Interdecadal variability of the East Asian winter monsoon and its possible links to global climate change. *J. Meteor. Res.*, **28**, 693–713, https://doi.org/10.1007/s13351-014-4046-y.

Feng, J., L. Wang, W. Chen, S. K. Fong, and K. C. Leong, 2010: Different impacts of two types of Pacific Ocean warming on Southeast Asian rainfall during boreal winter. *J. Geophys. Res.*, **115**, D24122, https://doi.org/10.1029/2010JD014761.

——, W. Chen, and Y. Li, 2016: Asymmetry of the winter extratropical teleconnections in the Northern Hemisphere associated with two types of ENSO. *Climate Dyn.*, **48**, 2135–2151, https://doi.org/10.1007/s00382-016-3196-2.

Gao, H., 2009: China's snow disaster in 2008, who is the principal player? *Int. J. Climatol.*, **29**, 2191–2196, https://doi.org/10.1002/joc.1859.

Geng, X., W. Zhang, M. F. Stuecker, and F. F. Jin, 2017: Strong subseasonal wintertime cooling over East Asia and northern Europe associated with super El Niño events. *Sci. Rep.*, **7**, 3770, https://doi.org/10.1038/s41598-017-03977-2.

Guo, L., C.-W. Zhu, B.-Q. Liu, and S.-M. Ma, 2018: Subseasonal variation of winter rainfall anomalies over South China during the mature phase of super El Niño events. *Atmos. Ocean. Sci. Lett.*, **11**, 396–403, https://doi.org/10.1080/16742834.2018.1505404.

Guo, S., and R. Wu, 2019: Contribution of El Niño amplitude change to tropical Pacific precipitation decline in the late 1990s. *Atmos. Ocean. Sci. Lett.*, **12**, 355–360, https://doi.org/10.1080/16742834.2019.1633230.

Hao, X., and S. He, 2017: Combined effect of ENSO-like and Atlantic multidecadal oscillation SSTAs on the interannual variability of the East Asian winter monsoon. *J. Climate*, **30**, 2697–2716, https://doi.org/10.1175/JCLI-D-16-0118.1.

——, ——, H. Wang, and T. Han, 2019: Quantifying the contribution of anthropogenic influence to the East Asian winter monsoon in 1960–2012. *Atmos. Chem. Phys.*, **19**, 9903–9911, https://doi.org/10.5194/acp-19-9903-2019.

He, S., and H. Wang, 2013: Oscillating relationship between the East Asian winter monsoon and ENSO. *J. Climate*, **26**, 9819–9838, https://doi.org/10.1175/JCLI-D-13-00174.1.

Held, I. M., M. Ting, and H. Wang, 2002: Northern winter stationary waves: Theory and modeling. *J. Climate*, **15**, 2125–2144, https://doi.org/10.1175/1520-0442(2002)015<2125:NWSWTA>2.0.CO;2.

Hsu, H.-H., and S.-M. Lin, 2007: Asymmetry of the tripole rainfall pattern during the East Asian summer. *J. Climate*, **20**, 4443–4458, https://doi.org/10.1175/JCLI4246.1.

Huang, B., and Coauthors, 2017: Extended Reconstructed Sea Surface Temperature, version 5 (ERSSTv5): Upgrades, validations, and intercomparisons. *J. Climate*, **30**, 8179–8205, https://doi.org/10.1175/JCLI-D-16-0836.1.

Jhun, J.-G., and E.-J. Lee, 2004: A new East Asian winter monsoon index and associated characteristics of the winter monsoon. *J. Climate*, **17**, 711–726, https://doi.org/10.1175/1520-0442(2004)017<0711:ANEAWM>2.0.CO;2.

Kalnay, E., and Coauthors, 1996: The NCEP/NCAR 40-Year Reanalysis Project. *Bull. Amer. Meteor. Soc.*, **77**, 437–471,

https://doi.org/10.1175/1520-0477(1996)077<0437:TNYRP>2.0.CO;2.

Kiritani, K., 2007: The impact of global warming and land-use change on the pest status of rice and fruit bugs (Heteroptera) in Japan. *Global Change Biol.*, **13**, 1586–1595, https://doi.org/10.1111/j.1365-2486.2007.01397.x.

Li, Y., and S. Yang, 2010: A dynamical index for the East Asian winter monsoon. *J. Climate*, **23**, 4255–4262, https://doi.org/10.1175/2010JCLI3375.1.

Lin, C.-Y., S.-C. C. Lung, H.-R. Guo, P.-C. Wu, and H.-J. Su, 2009: Climate variability of cold surge and its impact on the air quality of Taiwan. *Climatic Change*, **94**, 457–471, https://doi.org/10.1007/s10584-008-9495-9.

Liu, B., and C. Zhu, 2020: Diverse impacts of the Siberian high on surface air temperature in Northeast China during boreal winter. *Int. J. Climatol.*, **40**, 594–603, https://doi.org/10.1002/joc.6199.

Liu, J., J. A. Curry, H. Wang, M. Song, and R. M. Horton, 2012: Impact of declining Arctic sea ice on winter snowfall. *Proc. Natl. Acad. Sci. USA*, **109**, 4074–4079, https://doi.org/10.1073/pnas.1114910109.

Lü, Z., S. He, F. Li, and H. Wang, 2018: Impacts of the Autumn Arctic sea ice on the intraseasonal reversal of the winter Siberian high. *Adv. Atmos. Sci.*, **36**, 173–188, https://doi.org/10.1007/s00376-017-8089-8.

McPhaden, M. J., T. Lee, and D. McClurg, 2011: El Niño and its relationship to changing background conditions in the tropical Pacific Ocean. *Geophys. Res. Lett.*, **38**, L15709, https://doi.org/10.1029/2011GL048275.

Neale, R. B., and Coauthors, 2012: Description of the NCAR Community Atmosphere Model (CAM 5.0). NCAR Tech. Note NCAR/TN-486 +STR, 274 pp., http://www.cesm.ucar.edu/models/cesm1.0/cam/docs/description/cam5_desc.pdf.

North, G. R., T. Bell, R. Cahalan, and F. Moeng, 1982: Sampling errors in the estimation of empirical orthogonal functions. *Mon. Wea. Rev.*, **110**, 699–706, https://doi.org/10.1175/1520-0493(1982)110<0699:SEITEO>2.0.CO;2.

Ogata, T., S.-P. Xie, A. Wittenberg, and D.-Z. Sun, 2013: Interdecadal amplitude modulation of El Niño–Southern Oscillation and its impact on tropical Pacific decadal variability. *J. Climate*, **26**, 7280–7297, https://doi.org/10.1175/JCLI-D-12-00415.1.

Si, D., Q. Li, Y. Liu, Z. Wang, Y. Yuan, and D. Wang, 2014: Possible causes for the anomalous weak East Asian winter monsoon in 2013/14. *Meteor. Mon.*, **42**, 981–987.

——, L. Ma, P. Wang, Y. Wang, Y. Nie, and L. Sun, 2016: Anomalous activity of Arctic Oscillation in winter 2015/2016 and its impact on temperature in China. *Meteor. Mon.*, **42**, 892–897.

Song, L., L. Wang, W. Chen, and Y. Zhang, 2016: Intraseasonal variation of the strength of the East Asian trough and its climatic impacts in boreal winter. *J. Climate*, **29**, 2557–2577, https://doi.org/10.1175/JCLI-D-14-00834.1.

Takaya, K., and H. Nakamura, 2005: Mechanisms of intraseasonal amplification of the cold Siberian high. *J. Atmos. Sci.*, **62**, 4423–4440, https://doi.org/10.1175/JAS3629.1.

Tian, B., and K. Fan, 2020: Different prediction skill for the East Asian winter monsoon in the early and late winter season. *Climate Dyn.*, **54**, 1523–1538, https://doi.org/10.1007/s00382-019-05068-6.

Timmermann, A., and Coauthors, 2018: El Niño–Southern Oscillation complexity. *Nature*, **559**, 535–545, https://doi.org/10.1038/s41586-018-0252-6.

Wang, B., R. Wu, and X. Fu, 2000: Pacific–East Asian teleconnection: How does ENSO affect East Asian climate? *J. Climate*, **13**, 1517–1536, https://doi.org/10.1175/1520-0442(2000)013<1517:PEATHD>2.0.CO;2.

Wang, D., A. Wang, L. Xu, and X. Kong, 2020: The linkage between two types of El Nino events and summer streamflow over the Yellow and Yangtze River basins. *Adv. Atmos. Sci.*, **37**, 160–172, https://doi.org/10.1007/s00376-019-9049-2.

Wang, D. Q., B. Zhou, C. Sun, Y. Yuan, Y. Liu, and P. Wang, 2013: Features and possible causes for East Asian winter monsoon in 2012/13. *Meteor. Mon.*, **39**, 930–937.

——, T. Cui, D. Si, X. Shao, Q. Li, and C. Sun, 2015: Features and possible causes for East Asian winter monsoon in 2014/15. *Meteor. Mon.*, **41**, 907–914.

Wang, H., and S. He, 2012: Weakening relationship between East Asian winter monsoon and ENSO after mid-1970s. *Chin. Sci. Bull.*, **57**, 3535–3540, https://doi.org/10.1007/s11434-012-5285-x.

Weng, H., K. Ashok, S. K. Behera, S. A. Rao, and T. Yamagata, 2007: Impacts of recent El Niño Modoki on dry/wet conditions in the Pacific rim during boreal summer. *Climate Dyn.*, **29**, 113–129, https://doi.org/10.1007/s00382-007-0234-0.

——, S. K. Behera, and T. Yamagata, 2009: Anomalous winter climate conditions in the Pacific rim during recent El Niño Modoki and El Niño events. *Climate Dyn.*, **32**, 663–674, https://doi.org/10.1007/s00382-008-0394-6.

Wu, B., and J. Wang, 2002: Winter Arctic Oscillation, Siberian high and East Asian winter monsoon. *Geophys. Res. Lett.*, **29**, 1897, https://doi.org/10.1029/2002GL015373.

——, K. Yang, and J. A. Francis, 2016: Summer Arctic dipole wind pattern affects the winter Siberian high. *Int. J. Climatol.*, **36**, 4187–4201, https://doi.org/10.1002/joc.4623.

Wu, J., and X. Gao, 2013: A gridded daily observation dataset over China region and comparison with the other datasets. *Chin. J. Geophys.*, **56**, 1102–1111, https://doi.org/10.6038/cjg20130406.

Wu, R., Z. Hu, and B. P. Kirtman, 2003: Evolution of ENSO-related rainfall anomalies in East Asia. *J. Climate*, **16**, 3742–3758, https://doi.org/10.1175/1520-0442(2003)016<3742:EOERAI>2.0.CO;2.

Xiang, B., and B. Wang, 2013: Mechanisms for the advanced Asian summer monsoon onset since the mid-to-late 1990s. *J. Climate*, **26**, 1993–2009, https://doi.org/10.1175/JCLI-D-12-00445.1.

Xie, S.-P., Y. Du, G. Huang, X.-T. Zheng, H. Tokinaga, K. Hu, and Q. Liu, 2010: Decadal shift in El Niño influences on Indo–western Pacific and East Asian climate in the 1970s. *J. Climate*, **23**, 3352–3368, https://doi.org/10.1175/2010JCLI3429.1.

Xu, K., Q.-L. Huang, C.-Y. Tam, W. Wang, S. Chen, and C. Zhu, 2018: Roles of tropical SST patterns during two types of ENSO in modulating wintertime rainfall over southern China. *Climate Dyn.*, **52**, 523–538, https://doi.org/10.1007/s00382-018-4170-y.

Xu, X., F. Li, S. He, and H. Wang, 2018: Subseasonal reversal of East Asian surface temperature variability in winter 2014/15. *Adv. Atmos. Sci.*, **35**, 737–752, https://doi.org/10.1007/s00376-017-7059-5.

Xue, F., X. Dong, and F. Fan, 2018: Anomalous western Pacific subtropical high during El Niño developing summer in comparison with decaying summer. *Adv. Atmos. Sci.*, **35**, 360–367, https://doi.org/10.1007/s00376-017-7046-x.

Yeh, S. W., J. S. Kug, B. Dewitte, M. H. Kwon, B. P. Kirtman, and F. F. Jin, 2009: El Niño in a changing climate. *Nature*, **461**, 511–514, https://doi.org/10.1038/nature08316.

Yin, Z., Y. Li, and H. Wang, 2019: Response of early winter haze in the North China Plain to autumn Beaufort Sea ice. *Atmos. Chem. Phys.*, **19**, 1439–1453, https://doi.org/10.5194/acp-19-1439-2019.

Yu, M., C. Zhu, and N. Jiang, 2019: Subseasonal mode of cold and wet climate in South China during the cold season: A climatological view. *Atmos. Ocean. Sci. Lett.*, **12**, 73–79, https://doi.org/10.1080/16742834.2019.1568164.

Yu, S., and J. Sun, 2018: Revisiting the relationship between El Niño–Southern Oscillation and the East Asian winter monsoon. *Int. J. Climatol.*, **38**, 4846–4859, https://doi.org/10.1002/joc.5702.

Zhang, D., and W. Song, 2018: Northern Hemisphere atmospheric circulation characteristics in 2017/2018 winter and its impact on weather and climate in China. *Meteor. Mon.*, **44**, 969–976.

Zhang, J., W. Tian, Z. Wang, F. Xie, and F. Wang, 2015a: The influence of ENSO on northern midlatitude ozone during the winter to spring transition. *J. Climate*, **28**, 4774–4793, https://doi.org/10.1175/JCLI-D-14-00615.1.

——, ——, F. Xie, Y. Li, F. Wang, J. Huang, and H. Tian, 2015b: Influence of the El Niño Southern Oscillation on the total ozone column and clear-sky ultraviolet radiation over China. *Atmos. Environ.*, **120**, 205–216, https://doi.org/10.1016/j.atmosenv.2015.08.080.

Zhang, T., and Y. Huang, 2012: Impacts of climate change and inter-annual variability on cereal crops in China from 1980 to 2008. *J. Sci. Food Agric.*, **92**, 1643–1652, https://doi.org/10.1002/jsfa.5523.

Zhong, W., Z. Yin, and H. Wang, 2019: The relationship between anticyclonic anomalies in northeastern Asia and severe haze in the Beijing–Tianjin–Hebei region. *Atmos. Chem. Phys.*, **19**, 5941–5957, https://doi.org/10.5194/acp-19-5941-2019.